

A more precise way to localize animals using drones

Nathan T. Hui¹ | Eric K. Lo¹ | Jen B. Moss^{2,3} | Glenn P. Gerber⁴ |
Mark E. Welch² | Ryan Kastner⁵ | Curt Schurgers⁶

¹Engineers for Exploration, UC San Diego, La Jolla, California, USA

²Department of Biological Sciences, Mississippi State University, Mississippi State, Mississippi, USA

³School of Zoology, University of Tasmania, Hobart, Australia

⁴San Diego Zoo Wildlife Alliance, Beckman Center for Conservation Research, Escondido, California, USA

⁵Engineers for Exploration, Computer Science and Engineering, UC San Diego, La Jolla, California, USA

⁶Engineers for Exploration, Electrical and Computer Engineering, UC San Diego, La Jolla, California, USA

Correspondence

Nathan T. Hui, Engineers for Exploration, UC San Diego, La Jolla, CA 92093, USA.
Email: nthui@eng.ucsd.edu

Funding information

National Science Foundation, Grant/Award Numbers: CNS-1544757, CNS-1560162, CNS-1852403; Qualcomm Institute at UC San Diego; UC San Diego Frontiers of Innovation Scholars Program; San Diego Zoo Institute for Conservation Research; Mississippi State University; Rufford Foundation

Abstract

Radio telemetry is a commonly used technique in conservation biology and ecology, particularly for studying the movement and range of individuals and populations. Traditionally, most radio telemetry work is done using handheld directional antennae and either direction-finding and homing techniques or radio-triangulation techniques. Over the past couple of decades, efforts have been made to utilize unmanned aerial vehicles to make radio-telemetry tracking more efficient, or cover more area. However, many of these approaches are complex and have not been rigorously field-tested. To provide scientists with reliable quality tracking data, tracking systems need to be rigorously tested and characterized. In this paper, we present a novel, drone-based, radio-telemetry tracking method for tracking the broad-scale movement paths of animals over multiple days and its implementation and deployment under field conditions. During a 2-week field period in the Cayman Islands, we demonstrated this system's ability to localize multiple targets simultaneously, in daily 10 min tracking sessions over a period of 2 weeks, generating more precise estimates than comparable efforts using manual triangulation techniques.

KEYWORDS

aerial robotics, environmental monitoring, exploration, rotorcraft

1 | INTRODUCTION

In conservation biology and ecology, tracking individual animals is invaluable for understanding how they interact with other animals, humans, and their environment. It is critical for validating species migration and interaction models in the fields of integrative and experimental biology (Allen & Singh, 2016; Harris et al., 1990; Kenward, 2007; Lascelles et al., 2016; Millspaugh & Marzluff, 2009). The size of many animals, however, often limits the techniques that may be utilized. For instance, satellite and global positioning system (GPS) tags are not yet as useful to movement studies for small animals, as these tags are expensive and often too large to fit animals such as reptiles, insects, and small birds. Other remote sensing technologies such as subdermal implants and

ultrahigh bandwidth ranging radio, are either too short-range, or not compact/efficient enough for tracking small animals. As a result, tracking using very high frequency (VHF) tags that continuously transmit a very short ping remain a valuable technique in ecological and conservation studies (Kays et al., 2011; Wikelski et al., 2007). In particular, VHF tags weighing 1 g or less and less than 1 mm in diameter are used to study the movement of small animals over the span of days or weeks, often over kilometers of distance.

The most popular tracking techniques to use with VHF tags are homing/radio direction-finding (RDF) and triangulation, both done typically with a Yagi antenna with a beamwidth of 4–20°. However, both techniques require a radio frequency (RF) line of sight to the transmitter which may not be feasible in some terrain such as slot canyons or hills.

Further, reflected signals can generate an error in positioning estimates. In addition, the homing/RDF technique requires users to walk in the direction of the signal to locate transmitters, which can become infeasible due to terrain and vegetation. Triangulation is generally preferred in such circumstances. Triangulation requires three separate measurements, ideally from different sides of the transmitter, reducing the need to move on foot through dense vegetation. However, triangulation tends to be less accurate due to the lack of precision in determining the signal-bearing (Mech, 1986; White & Garrott, 2012). Both of these methods also require the use of an impractically large antenna, approximately 0.5 m wide, so moving through difficult terrain is very difficult (Mech, 1986). In addition, of these methods, only triangulation can track multiple signals at the same time.

The easiest solution to avoid the obstacles of terrain and vegetation is to escape the environment in which these obstacles exist. In general, dense foliage or impassable terrain only affect land mobility—it does not affect aerial mobility. Thus, flying sensors over these areas provide an avenue for avoiding the obstacles presented by foliage and terrain, which are common obstacles in many biological and ecological field sites.

Some scientists have used manned aircraft to conduct wildlife tracking surveys. In general, these surveys are conducted by attaching directional antennae to the outside of a fixed-wing aircraft and flying RDF missions. Much like conducting RDF tracks on foot, this requires RF line of sight, however, this is much easier to manage because the receiver is now in the air, and so has RF line of sight to far more places on the ground. In addition, while dense vegetation limits the ability of the researchers to visually verify a target from overhead, flying overcomes the inability to physically track subjects on foot (Mech, 1986; White & Garrott, 2012).

The primary issue with manned aircraft tracking surveys is the increased cost and logistics needed to support such surveys. Fixed-wing aircraft surveys require pilots, aircraft, fuel, and maintenance, among other logistics and support items. Survey time would be limited to the aircraft's loiter time minus transit time from the support airfield to the survey area, potentially making manned aircraft surveys in particularly remote areas infeasible from a cost and logistics standpoint (Mech, 1986).

Over the past decade, small unmanned aerial vehicles have developed to the point that they are now inexpensive and robust enough to use as low-cost sensor platforms for scientific research. Drones have been applied to a variety of ecological survey applications, including aerial mapping and wildlife tracking. In addition, software-defined radios (SDRs), which allow us to rapidly reconfigure a radio and receive a large swath of the radio spectrum simultaneously, have matured to the point that there are sufficiently low cost, robust, and lightweight radios commercially available that can be used as part of a UAV sensor payload that can track multiple animals simultaneously (Gottwald et al., 2019; Nabeel & Bloessl, 2016; Nguyen et al., 2019; Santos et al., 2014; Vonehr et al., 2016; Webber et al., 2017).

Over the past few years, several researchers have developed prototype autonomous drone tracking systems for tracking VHF

transmitters. The advantage of using drones is that they can move across the survey area faster and with more precision, and collect more informative and precise measurements than a human with an analog receiver. This allows us to use more information to generate a more precise estimate. In addition, using an SDR allows drones to track multiple transmitters simultaneously, allowing a single drone flight to be more efficient. These systems generally approach the estimation problem in one of two ways—bearing-based (Posch & Sukkarieh, 2009; Bayram et al., 2018; Cliff et al., 2015, 2018; Dressel & Kochenderfer, 2018; Vonehr et al., 2016) and range-based (Jensen & Chen, 2013; Korner et al., 2010; Santos et al., 2014; Soriano et al., 2009).

Bearing-based estimation seeks to emulate the traditional terrestrial approaches with a drone. These systems take one of two approaches to determine the bearing to the transmitter: using either a highly directional antenna and rotating to detect the signal or an antenna array that can measure the direction of arrival of the signal. Because of this, bearing-based estimation typically requires complex antenna or receiver configurations, and are typically physically larger. This affects the suitability of such systems for field use, as larger systems are more difficult to utilize in the field, and often require more maintenance.

Range-based estimation, on the other hand, utilizes the precision with which we can measure the signal strength of the received signal and the relationship between received signal strength and distance to the transmitter. This uses a much smaller and simpler antenna configuration, which increases its usability and robustness while decreasing the cost and complexity of the system. Some range-based approaches attempt to take the directionality of the antenna into account by mapping the directionality of the antenna to the range estimates, which can assist in increasing the precision of the final position estimate (Posch & Sukkarieh, 2009; Cliff et al., 2018).

Many of the recent bearing-based and range-based systems use estimation approaches such as particle filters (Posch & Sukkarieh, 2009; Korner et al., 2010; Nguyen et al., 2019), grid filters (Cliff et al., 2015; Dressel & Kochenderfer, 2018), and Kalman filters (Jensen & Chen, 2013). These are all variations of Bayesian estimation, and require an accurately characterized probability distribution of the source of noise from observations and sensors to determine the probability of a particular estimate being correct.

Because the main challenge in evaluating these systems is that the performance in real-world field conditions is significantly different from those in carefully controlled test scenarios, few, if any, of the recent prototype drone tracking systems have data on their performance under field conditions. A survey of the most mature systems (Cliff, Dressel, and Nguyen) found evidence for fewer than 30 field trials (Cliff et al., 2018; Dressel & Kochenderfer, 2018; Nguyen et al., 2019). This lack of field testing results in a major impediment to determining the real-world usability of such systems in scientific research. Of these, the most precise system estimates the location to a 5 m cell, but only gives a 50% certainty that the transmitter is located within that cell. The remaining two systems (Cliff and Nguyen) generate estimates within 20 m (Cliff et al., 2018; Nguyen et al., 2019). Both Dressel and Nguyen quote localization times of less than 5 min for trial flights, however, these were done

with the copter starting within the detection range of the transmitter, and not in field conditions, where the drone often initiates operations far from the target animal (Dressel & Kochenderfer, 2018; Nguyen et al., 2019). Note that all systems presented in this paper require foreknowledge of the general location of the transmitter to function properly, as the fully autonomous systems require that they fly to within detection range before beginning their tracking, and our partially autonomous system requires the search area to be planned over the estimated detection range.

In 2013, the San Diego Zoo Institute for Conservation Research (SDZICR) partnered with Engineers for Exploration, a student-centered research group at UC San Diego, to explore the potential systems for automating the radio tracking of iguana hatchlings in the Dominican Republic leveraging existing VHF technologies. The initial results on this system were published in 2014 by dos Santos et al. (2014). This represented a proof-of-concept system in a controlled test environment. In 2015, we deployed an initial field-deployable system to the Dominican Republic that corrected the signal processing presented by dos Santos and enabled using multiple measurements of the transmitter's signal strength to generate a heatmap, and thus generate an estimate of the transmitter location, and over the course of several days, a track of the animal's movement in field conditions. This iteration of the proof-of-concept system showed that our approach worked, but required too much maintenance to be a valuable tool in the field. In 2016 and 2017, an improved system that further expanded the capability of the signal acquisition and processing, as well as added the position estimation and full systems integration, was deployed in the Cayman Islands in conjunction with SDZICR, Mississippi State University, and the Cayman Islands Department of Environment to track nesting female iguanas and hatchling iguanas dispersing from their natal sites.

During the deployment in 2017, we were able to compare the performance of the drone-based tracking system to that of trained field ecologists. Unlike many other comparative studies, which pit drone systems against field ecologists in isolated trials, we were able to evaluate the system with the time and resource constraints of an actual research expedition. This provides a relevant and applicable metric from the perspective of the end-user, which assisted in determining that this can be an effective tool for field biologists, as well as validates the original system concept described by dos Santos et al.

In this paper, we will describe this system, the results of those real-world field deployments, and our analysis of the data. We believe it shows our system is a robust and rugged solution that uses range-based measurement to drive model-based estimation of the target. This system, during extended field deployment, demonstrated performance on par with traditional triangulation methods in terms of accuracy and outperforms traditional tracking methods in terms of measurements per day. We will first present the architecture and methodology from an algorithmic perspective for the drone-based tracking system, then the specific implementation and realization of the system used, and finally, the qualitative and quantitative performance metrics from in-field validation and a comparison of this system with other solutions. The contribution of this study is the

presentation of a complete drone-based tracking system that has been tested and validated in a multiday remote field expedition.

2 | SYSTEM OVERVIEW

Our drone-based tracking system is comprised of two independent subsystems—the drone (flight platform), and the sensor payload. We elected to make this separation to permit the future move to different flight platforms, or even different mobility platforms such as vehicles and balloons, and to ensure that failures in the sensor payload do not propagate into the flight platform and cause further issues.

We chose to use received signal strength to drive our estimation of the transmitter location for its simplicity and robustness. Determining the signal strength of a ping simply requires an analog to digital converter. Determining the distance from the ping to the transmitter then requires relating the received signal strength of a transmission to the distance to the transmitter. This is independent of the directionality of the antenna, transmission power, and system gain. In addition, this approach benefits from having an antenna with as little directionality as possible.

To accomplish this, we further break the payload system down into several subsystems: antenna, low noise amplifier (LNA), SDR, GPS/compass, on-board computer, data storage, processing pipeline, and visualization tools. We show the overall system architecture in Figure 1.

In this system, the antenna receives the RF ping from the transmitter. This signal is amplified by the LNA, which is then amplified yet again and digitized by the SDR. The on-board computer records this digital signal from the SDR, along with GPS and heading information from the GPS/compass unit, and stores all of this into external storage. The recorded data feed into the processing pipeline, which detects all pings, then estimates the location and certainty of the transmitter location. This information can then be visualized in geospatial information system (GIS) software. The following sections will present the wildlife transmitters themselves, and



FIGURE 1 Left: Payload system diagram. The antenna and LNA feed radio signals to the SDR. The on board computer receives the radio signal from the SDR, GPS position from the GPS/compass, and commands from the UI. All of this is stored on the local data storage. Right: 3DR Solo (discontinued in 2016) with radio tracking payload. GPS, global positioning system; LNA, low noise amplifier; SDR, software defined radio; UI, user interface [Color figure can be viewed at wileyonlinelibrary.com]

then the detection and estimation process. The specific hardware implementation is presented in Section 3, and the testing and performance results are presented in Section 5.

2.1 | Wildlife transmitters

For the 2017 deployment, we were tracking VHF wildlife transmitters, in particular, the Holohil BD-2 and PD-2 transmitters.¹ However, our methodology is independent of the specific choice of transmitter. Figure 2 shows the BD-2 transmitter in detail and attached to a *Cyclura cornuta* hatchling in the Dominican Republic. These transmitters are all very small, in general less than 2 g. As a result of their size and weight, they do not have a very high output power, on the order of 1–10 mW. These are typically configured to transmit a 10–20 ms pulse on a specific frequency every 1–2 s in a way that maximizes their battery life over the intended field life.

One of the challenges of working with these transmitters is the variability in transmission characteristics. Because of the simplicity of these devices, the transmit frequency will vary as the battery voltage decreases and the temperature varies. Field notes suggest a drift due to battery depletion of as much as 1 kHz over a period of 1 week. Lastly, as the transmitter ages, the transmission power decreases, which makes these transmitters more difficult to detect. However, all of these issues are addressed in our signal processing, which is discussed later.

2.2 | Path planning

Our system estimates the location of the transmitter by using measurements of the ping's signal strength in a survey area to estimate where the loudest point should be, and thus where the transmitter would be located. However, since we do not know the transmitter's exact location before flying the mission and the transmitter location is being estimated on a separate computer, we need to maximize the efficiency of the flight path in terms of area covered.

Given the constraints above, our flight path must maximize its coverage of an area while still loitering above each point on the ground long enough to determine whether or not there is a ping at that location. Fundamentally, we are attempting to determine the location of the transmitter by mapping out the transmitter's signal strength over the search area. We develop our search area by evaluating our best guess of where the transmitter currently is. Often, we use a combination of last known position, as well as quick verification using traditional tracking equipment to verify that the transmitter is roughly where we expect. This usually consists of taking a quick bearing with a handheld directional antenna to confirm that the transmitter is in the same direction as the search area.

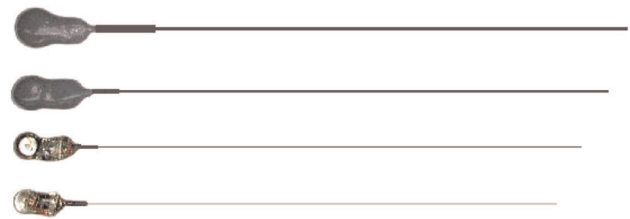


FIGURE 2 Holohil BD-2 wildlife transmitters, in detail and attached to *Cyclura cornuta* [Color figure can be viewed at wileyonlinelibrary.com]

In some cases, we find that the animal had started moving significant distances—in these cases, we use a directional antenna to find the bearing along which the animal is located, drive to a convenient launch point, and set up a search area to search along that bearing as far as possible. This maximizes the coverage of the area that we think the animal is in. While the search area could be defined without using the directional antenna to provide an initial guess, operationally, using the directional antenna to inform the initial search area reduces the amount of effort spent searching areas that are known to not contain a transmitter.

The simplest and most efficient flight path for surveying a convex polygon is what is known as a lawnmower pattern. This pattern consists of evenly spaced lanes oriented parallel to the survey area's longest axis, with the drone flying up one lane and down the next. An example of this is shown in Figure 5. We select our survey speed to be 5 m/s based on our understanding of the minimum effective range of the payload, and the most efficient speed for the flight system. Based on a worst-case detection range of 30 m and a lane spacing of 30 m, if we fly at our minimum speed of 5 m/s, we can, in the worst-case scenario of flying a line directly over the transmitter, with adjacent lanes just out of range of the transmitter, detect eight pings. In the best-case scenario of flying two lanes equidistant from the transmitter, we can expect as many as 13 pings. This choice of lane width maximizes the area that we can survey while still ensuring that we have enough measurements to estimate the transmitter location. Note that the worst-case scenario occurs when searching for

¹<http://www.holohil.com/>

transmitters with depleted batteries. In normal operations, transmitters with fresh batteries have a detection range of nearly 100 m, as depicted in later in Figure 5. This results in significantly more than 13 pings per mission that we can use to estimate the transmitter location. During our deployment, we regarded missions measuring fewer than 20 pings to be marginal with respect to the quality of data, and often reflect those missions or manually verified the result.

In general, the survey speed is slow enough that we can guarantee more than four detections in the worst-case scenario. We can, in principle, generate solutions for transmitter locations where we only detect them on one lane if the detection radius is actually smaller than we estimate. In theory, we can still generate an estimation for the actual location of the transmitter, but it will have some ambiguity as to which side of the survey line the transmitter is on. However, this is an acceptable tradeoff, as transmitters that have decayed to this state are likely also very difficult for the researchers to detect, and likely need to be replaced. This method is tolerant of underestimation of the system's ping detection radius since a detection radius larger than our estimate guarantees that the transmitter will be heard across at least two lanes, and provides more data, thus improving the estimate. We further expand on the way we can recognize degenerate solutions caused by insufficient data in Section 2.6.

In total, the selected search area is selected based on the nominal lawnmower pattern to evenly cover the area around the initial guess of the transmitter location, the nominal survey speed, the total flight endurance for the vehicle, and finally, situational routing. This is specific to each individual area surveyed, and can result in a 100×100 m area to a 600×600 m area, depending on the launch location, survey area visibility, prevailing winds, battery performance, desired coverage, local obstacles, survey approach, and procedural constraints around operating the aircraft. Procedural constraints may include control link range if fully autonomous flight is not permitted, visual range if beyond visual range operation is not permitted, airspace restrictions, overflight restrictions, weather and traffic avoidance.

2.3 | Dipole antenna

Our system uses the change of received signal strength as the drone moves around the transmitter to determine the location of the transmitter. For this to be effective yet simple, we need an omni-directional antenna so that the received signal strength is independent of the orientation of the survey platform.

We elected to use a dipole antenna because of its near omni-directional characteristics. In its horizontal orientation, with the nulls pointed to the horizon, the projected beam pattern on the ground is nearly circular, which eliminates attenuation of the target signal due to directionality. This allows us to treat the received power of the transmit signal as a proxy for the distance between the transmitter and receiver. This omni-directionality allows for a much simpler computational model, and opens up the possibility of using this exact sensor payload on a fixed-wing aircraft, where we cannot decouple the orientation of the antenna from the flight path of the aircraft.

In addition to its omni-directional characteristics, the dipole was measured to have a sufficiently wide bandwidth of 2 MHz. During our field testing, we found that the transmitters came on unique frequencies separated by as little as 15 kHz, spanning a total of 1 MHz. This is ideal for our purposes because it allows us to receive a wide variety of signals without significant losses. Since the radio tags are assigned unique frequencies for identification by the tag manufacturer, this can result in a significant range of frequencies that need to be received, which is handily covered by the 2 MHz bandwidth of the dipole antenna.

Additionally, because of the simplicity of the dipole antenna, the resulting design is lightweight, which permits its integration onto small drone platforms. This is particularly important due to the requirement that this be operable in field conditions, where the UAV will often be transported in a vehicle with a lot of additional equipment, or on foot through dense foliage.

2.4 | Radio receiver

To convert the analog RF signal to a digital signal we can process, we use a SDR. SDRs operate by first amplifying the induced voltage in the antenna to measurable levels, then shifting the signal from the center frequency f_c to baseband (0 Hz). This signal is then sampled at a sampling frequency f_s in both the real (in-phase) and complex (quadrature) components to generate the digital IQ signal that is then passed to the onboard computer for processing.

We specifically use an SDR as opposed to the conventional analog receiver that is commonly used in radio-tracking because the SDR allows us to receive multiple frequencies simultaneously, allowing for the tracking of multiple transmitters during any given survey. In addition, the SDR allows us to control the center frequency, sampling rate, gain, and resolution via software commands. This allows us to rapidly reconfigure the system to scan for different types of transmitters (VHF or UHF) without making any hardware changes, whereas using a conventional receiver would require a new receiver for VHF and UHF, and even potentially different receivers for different frequencies within VHF/UHF ranges, as conventional receivers are only capable of tuning to a range of frequencies approximately 4 MHz wide.

To ensure that the bandwidth of the SDR covers the frequencies of the transmitters we are interested in, and to avoid the DC spike characteristic of SDRs, we selected $f_s = 2 \text{ MS s}^{-1}$ and $f_c = 172.5 \text{ MHz}$. The SDR receives complex signal data, which allows us to determine the sign of frequencies, so the signal bandwidth is equivalent to the sampling frequency, thus allowing us to be able to receive frequencies from 171.5 to 173.5 MHz, which is the frequency range of our transmitters.

2.5 | Signal processing

To estimate the location of the transmitter, we need to first identify and measure the individual pings as received by the SDR. To process the RF data, we first extract the specific frequencies emitted by the

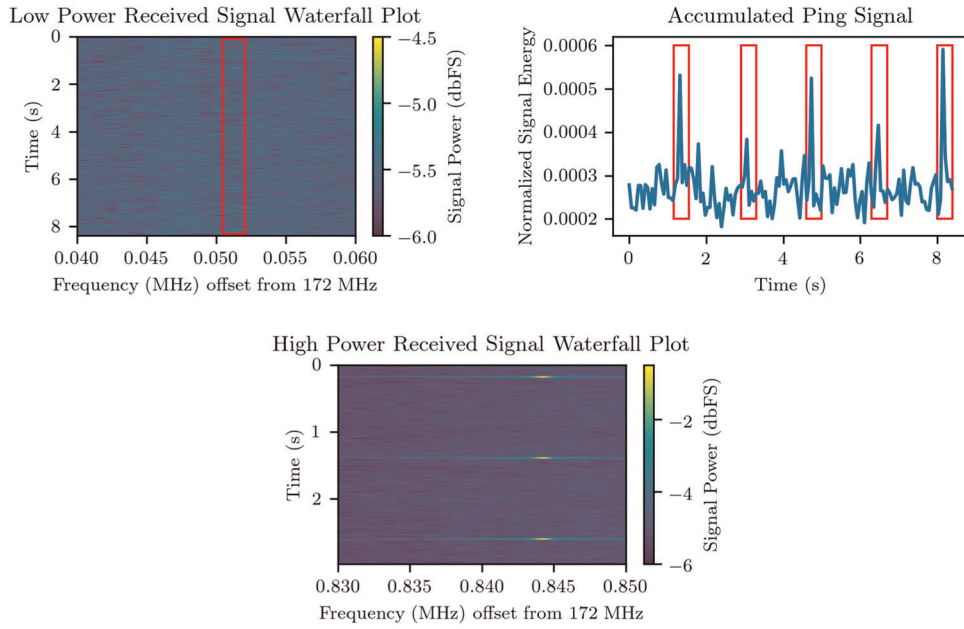


FIGURE 3 The High Power Signal Waterfall Plot shows three pings at 172.843 MHz, at approximately 0.1, 1.2, and 2.8 s, demonstrating how well signals can stand out. The red box in the center of the low power received signal waterfall plot of highlights the target frequency for a transmitter that is very far away. The red boxes in the accumulated ping signal plot identify the ping energy, showing how this technique can be used to enhance the signal to noise ratio [Color figure can be viewed at wileyonlinelibrary.com]

transmitters by calculating the Short-time Fourier Transform. The Short-time Fourier Transform is simply sequential Fourier Transforms of length n computed on a longer signal. This is commonly computed using the Fast Fourier Transforms (FFTs). FFTs of length n can be treated as a bank of n adjacent band-pass filters. The i th filter has a passband centered at $f_c + \left(\frac{i}{n}f_s\right)$ with width $\frac{f_s}{n}$, where i is in $\left[\frac{-n}{2}, \frac{n}{2}\right]$. We start by running an FFT over the entirety of the data to convert the time domain signal to a waterfall plot (time vs frequency vs amplitude), a sample of which is shown in Figure 3. We do an FFT of 4096 elements, which gives us a frequency resolution of roughly 500 Hz per bin ². Quantitative tests show that the transmitted signal has a bandwidth of less than 500 Hz, which results in us being able to positively identify each ping to the correct frequency. This also allows us to compensate for any frequency drift in the transmitter, as mentioned earlier. The resulting signal also has a much higher signal-to-noise ratio (SNR) as it is rejecting the remaining frequencies.

$$x[i] \in \mathbb{C} \quad (1)$$

$$X_f[k] = \mathcal{F}\{x[4096k: 4096(k+1) - 1]\}[f] \quad (2)$$

$$E[m] = \sum_{k=19m}^{19(m+1)-1} 10 \log_{10}(|X_f[k]|^2) \quad (3)$$

$$P[n] = \max\{E[37.5n], \dots, E[37.5(n+1) - 1]\} \times 25 \quad (4)$$

Once we have the waterfall plot, we accumulate 40 ms of power information for the frequency we are interested in, as shown in the right image in Figure 3. This is the measure of the energy in the signal over the 40 ms window, described by Equation (3). By accumulating over twice the width of the ping, we can better ensure that the estimated ping is covered by the window. This makes the pings,

which are otherwise not visible in the left image showing instantaneous power, visible in the right image. Finally, to identify each ping and measure the average received signal power, we simply identify the maximum energy in each 1.5 s window, effectively choosing the most energetic moment in each 1.5 s period (Equation 4). Since the transmitted signal has a roughly 1.5 s period, we assume that the loudest signal in the frequency in each 1.5 s window is the ping, if we heard the signal at all.

To generate an initial estimate of the transmitter location, we need to determine which of the signal data are actually pings. To do this, we take each ping and associate it with the nearest GPS measurement in time. To determine whether a ping was actually received or not, we lay a grid with 100 m spacing over all of the measurements. For each cell in the grid, we calculate the median received signal power. We then use the highest median received signal power as a threshold with which to select data to feed into the nonlinear least squares estimator.

2.6 | Location estimation

Once we identify pings, we fit them to a signal propagation model. We know that the power of a radio signal decays proportional to the inverse square of distance in a vacuum (Whitaker, 2005). In practice, the exponent for the path loss can vary depending on the environment, so we elect to use the model shown in Equation (5), where R_i is the received signal power for the i th measurement in dB, P is the transmit power in dB, L is the path loss in dB, n is the path loss exponent, $\mathbf{D}_i \in \mathbb{R}^3$ is the position of the i th measurement in m,

$\mathbf{T} \in \mathbb{R}^3$ is the transmitter location in m, and C represents additional system losses in dB (Gutierrez, 2008).

$$R_i = P - L = P - 10n \log_{10}(|\mathbf{D}_i - \mathbf{T}|) - C \tag{5}$$

$$k_1 = \frac{-1}{n} \tag{6}$$

$$k_2 = \frac{P - C}{n} \tag{7}$$

$$d_i = |\mathbf{D}_i - \mathbf{T}| = 10^{\frac{k_1 R_i + k_2}{10}} \tag{8}$$

Each measurement consists of the received signal strength R_i in dB and the drone's location $\mathbf{D}_i = (D_{ix}, D_{iy}, D_{iz})$ in meters from some fixed datum on the ground. Thus, our unknowns are P (transmit power), n (path loss exponent), \mathbf{T} (transmitter position), and C (additional system losses). To simplify the problem, we reparameterize Equation (5) with k_1 and k_2 , shown in Equations (6) and (7). We are then able to calculate d_i using Equation (8), which assumes the transmitter location (T_x, T_y) is on the ground ($T_z = 0$), which is a reasonable approximation in mostly flat terrain.

$$\begin{aligned} & \begin{bmatrix} \hat{k}_1 \\ \hat{k}_2 \\ \hat{T}_x \\ \hat{T}_y \end{bmatrix} \\ & = \arg \min_{k_1, k_2, T_x, T_y} \frac{1}{N} \sum_{i=1}^N \left| \sqrt{(T_x^2 - D_{ix}^2) + (T_y^2 - D_{iy}^2) + D_{iz}^2} - 10^{\frac{k_1 R_i + k_2}{10}} \right|^2 \end{aligned} \tag{9}$$

Since we are solving not only for the transmitter location in two dimensions, but also for the RF signal parameters in k_1 and k_2 , we have a model with four parameters. To find a solution for these parameters, we need at least four measurements, more if we wish to characterize the accuracy of our estimate. We then use a nonlinear least squares solver (`scipy.optimize.least_squares`) to find parameters that best fit the measurements. This is accomplished by

finding $\hat{k}_1, \hat{k}_2, \hat{T}_x, \hat{T}_y$ with Equation (9), which finds the minimum mean squared error estimate of the model parameters.

$$\begin{bmatrix} D_{ix} \\ D_{iy} \end{bmatrix} - \begin{bmatrix} \hat{T}_x \\ \hat{T}_y \end{bmatrix} \sim \mathcal{N} \left(10^{\frac{\hat{k}_1 R_i + \hat{k}_2}{10}}, \left(0.4 \times 10^{\frac{\hat{k}_1 R_i + \hat{k}_2}{10}} \right)^2 \right) \tag{10}$$

Once we estimate the model parameters, we still need to provide a measure of the precision of the estimate. To do this, we overlay an estimate of the probability of the transmitter position for each ping. This consists of a normal distribution centered on the distance calculated by the model parameters for that ping with a SD of 40% of the distance, rotated around the ping's receive location (Equation 10). Careful examination of our test results yielded this estimate as a good estimator of the precision of our path loss model. The hot spot resulting from the sum of all the pings represents a measure of the likelihood for the location of the transmitter. These distributions are shown graphically in Figure 4.

Figure 4 specifically shows an example with only three range estimates. In practice, we find that we have in excess of 10 range estimates per solution, which results in a much sharper distribution of confidence. This is a result of more data enforcing the estimated location. We show a practical example of this in Figure 5, where the estimated location and confidence distribution uses information from well over 30 measurements, resulting in a very small error distribution.

To generate a confidence interval for the estimate, we then take the contour of equal likelihood in which there is a 95% likelihood of containing the estimate, and take the maximum radius of that contour as the radial confidence interval of the estimated location. While this dilutes the precision of our estimate, it provides a conservative estimate of the actual precision of the location.

This graphical display of the precision of the estimate helps us to identify certain degenerate solutions. Such solutions can occur when all the data are essentially in a straight line, and there are multiple spatial solutions to the model. This shows up as two "hot spots" in the visualization. Another possible degenerate solution occurs when

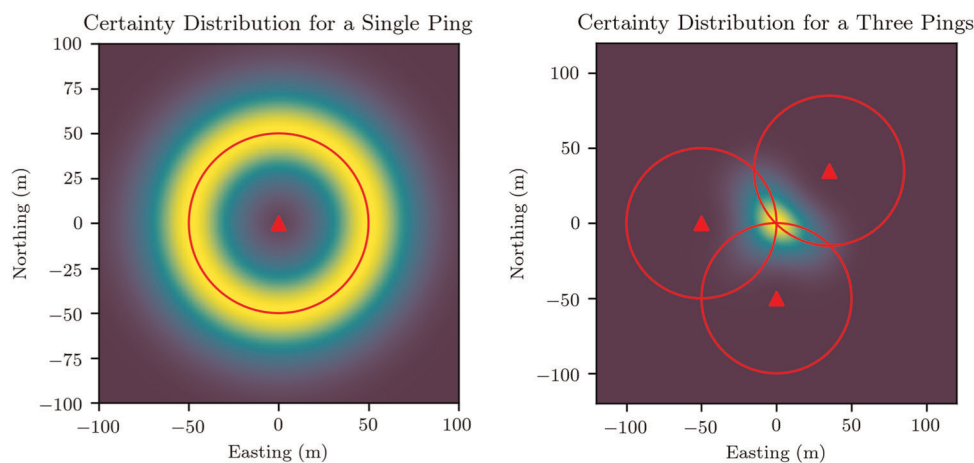


FIGURE 4 Spatial precision distributions. The left image shows the probability mass distribution of the possible locations from a single ping. The right image shows the probability mass distribution of the possible estimate locations from three pings. The red triangles denote the measurement location. The red circles denote the calculated distance for each measurement [Color figure can be viewed at wileyonlinelibrary.com]

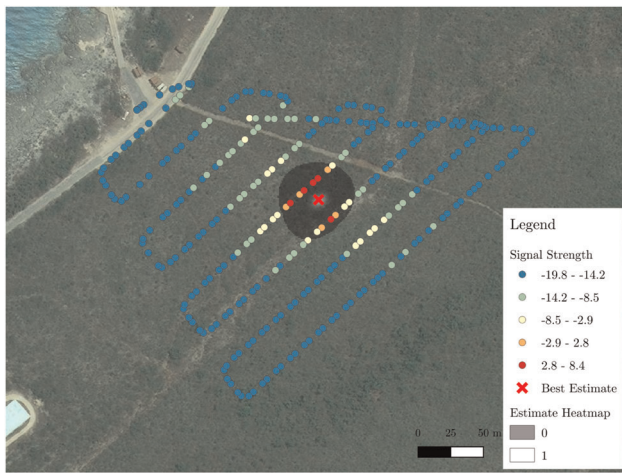


FIGURE 5 Mission 70 results, August 23, 2017 [Color figure can be viewed at wileyonlinelibrary.com]

the estimated range becomes very large with respect to the distance between measurements, such as when all measurements are spatially close and have little variance. This manifests as a larger and more dilute view of the single ping precision distribution. Thus, a valid set of measurements and calculated estimate looks most like the right-most image in Figure 4, albeit much smaller and more pronounced.

While other systems have used Bayesian estimation to solve for their estimate, we use a nonlinear least-squares solver to keep the system simpler and lighter. Bayesian estimation requires a prior characterization of the noise in the system, which can be impractical. In general, it is also more computationally expensive, requiring faster and more expensive computational hardware, thus increasing the overall cost of the system.

Our localization method assumes that the target is stationary during the measurements. However, this is not always true, as the subject animal may be moving around. Because we are using a least-squares solver, we are finding the location that has the highest likelihood of being the location that would have generated the recorded measurements. With a moving target, this effectively becomes a form of the mean location of the target during the recorded measurements. Given that our overall objective is to track the target animals moving over several days/weeks, this is an acceptable outcome, as we are still able to generate a track of gross movement.

2.7 | Visualization

We can visualize the data as GIS data, plotting the measurement locations by their respective signal strengths, a heatmap of all probable locations, as well as the most probable location. This is provided as a GeoTIFF image containing the probability map, and an ESRI Shapefile containing the most probable location and measurement points. This visualization and data format provides a nearly seamless method for scientists to incorporate our measurements into their work. An example of the resulting data visualization is shown in Figure 5.

Figure 5 provides the following information: flight path, measured signal strength, final estimate, and estimate precision. The flight path is marked by the dotted paths—the drone took off from the parking area in the northwest corner of the map, flew the lawnmower pattern, then returned directly home from the northeast corner of the search area. Each dot represents a location that the drone measured the signal strength at. Because our system at the time did not reject signal strength measurements from below the noise floor, the system does attempt to measure the signal strength of the noise. This is later rejected when selecting the data from which to generate the final estimate. Each signal strength measurement is colored according to its amplitude; we can see a hot spot where the red and orange dots are, which is intuitively where the transmitter is located. The final estimate is marked by the red X, and the likelihood map of that estimate is represented by the grey heatmap. Note that this heatmap is much sharper than the heatmap presented in Figure 4—this is because the heatmap in Figure 5 uses information from over 30 measurements to generate the final estimate, resulting in a much higher confidence.

3 | IMPLEMENTATION OVERVIEW

The system as described in Section 2 can be placed on any vehicle, so long as the platform has the appropriate payload capacity and maneuverability. In this section, we present the specific implementation of the system (Figure 1) as deployed on Little Cayman in 2017.

3.1 | Flight hardware

We elected to use the 3DR Solo² due to the clean user interface and small learning curve for operational use. The 3DR Solo eliminates any possibility of placing the aircraft into a non-GPS controlled mode, and minimizes the number of switches and buttons relevant to the mission. In conjunction with the 3DR Solo, we use a MacBook Air with a Windows install to run Mission Planner³ as our primary mission control ground station and mission planning software. We selected Mission Planner as it is the most mature mission control and planning software available for the ArduPilot family of UAV autopilots. The ground station connects to the 3DR Solo via the 3DR Solo's WiFi link, which is hosted on the 3DR Solo Controller.

Fundamentally, this system can be integrated with any flight platform capable of lifting the ≈ 300 g payload. Previous iterations of this system were deployed on platforms such as a DJI S800 and Tarot Ironman 650. In principle, so long as the vehicle can autonomously fly a preprogrammed flight pattern and lift the payload, this system ought to function, since the flight pattern can be modified to ensure that the aircraft spends enough time in the area of interest to gather enough signal measurements to produce a satisfactory estimate.

²Discontinued in 2016.

³<http://ardupilot.org/planner/>

3.2 | Software defined radio

We elected to use the USRP B200mini,⁴ which is a 1 × 1 SDR in a 83.3 × 50.8 × 8.4 mm form factor. This provides a high-performance SDR in a small and lightweight package, which is ideal for use on UAVs. This is combined with an LNA4ALL⁵ LNA, which provides 22 dB of gain in the VHF band, and helps provide the onboard computer with a high-quality radio signal.

3.3 | On-board computer

We elected to use the Intel Joule,⁶ which is a compact x86 single-board computer, as the onboard computer. The Intel Joule comes with a breakout board that exposes USB 3.0, hardware serial, general-purpose input/output (GPIO), and external storage. This allowed us to interface directly with the USRP, GPS unit, and external storage. In addition, the GPIO allowed us to interface with a custom user interface (UI) board, which provided a way for the user to signal the computer to start recording and to check the status of the various systems on board.

The Joule is configured to start a suite of monitoring software on boot, which allows it to monitor and manage the status of the various sensors and subsystems and display those on the UI board. This software suite is also responsible for starting the recording software and marshaling the data into the appropriate locations on an external storage device.

The Joule receives complex RF signal data from the USRP via the USRP Hardware Driver library. This is subsequently unpacked and stored to disk as sequential complex integers. It also receives GPS data from a Ublox M8N GPS module. All of this data is timestamped and recorded, along with metadata such as the SDR's sampling rate, center frequency, and amplifier gain. Signal processing and estimation is conducted postflight on a dedicated processing laptop.

4 | PERFORMANCE

In 2016 and 2017, we deployed the prototype drone tracking system on the island of Little Cayman, Cayman Islands in partnership with a team of iguana researchers from Mississippi State University and SDZICR to evaluate and demonstrate the capabilities of the system. For the 2017 deployment, we conducted near-continuous tracking operations for 2 weeks, tracking 22 individual transmitters with an average of 11 tracks per day.

These tracks were compared to triangulation methods where possible, and conducted in cooperation with the field researchers. We were able to generate a total of 152 scientific tracks, accruing a total of 13.5 h of flight time.

4.1 | Ground truth

In 2016, we deployed the prototype drone tracking system without the position estimation implementation to track known adult iguana locations (primarily iguanas on the side of the road, stationary in clearing, or in known burrows). These data showed that the signal amplitude heatmaps were a very good indicator of the transmitter location, and we and the researchers were able to pick out the transmitter location by eye. We were able to use this recorded data to develop and test the position estimation implementation, which showed that the estimates generated were within GPS accuracy (5–10 m).

In 2017, we were not able to gather as much ground truth data, due to the increased number of subjects to track, and because we were focusing on tracking iguana hatchlings. These hatchlings tended to travel through heavily brushed areas, thus inhibiting our ability to actually locate the animal and get a GPS reading on its location. However, on a couple of occasions, we were able to verify a few estimates using GPS, because the subject animals had moved to locations easily accessible from the roadside.

4.2 | Field utility

The overarching scientific goal of the radio-tracking study on Little Cayman was to characterize a poorly understood process in the life history of a critically endangered iguana species—natal dispersal (Moss et al., 2020). This would contribute to an improved understanding among conservation researchers of this cryptic early life stage, including how the behaviors exhibited by hatchlings may ultimately shape patterns of recruitment and admixture in otherwise stable adult populations. The principal investigators ambitiously aimed to track 28 hatchlings—14 brother–sister pairs—each for a period of approximately 4 weeks. A minimum of one transmitter location per day was desired to track animal movement patterns. Because hatchling iguanas are small and previous studies have shown that they are capable of rapid movements when dispersing (Knapp et al., 2010; Pérez-Buitrago & Sabat, 2007), tracking this many animals over a relatively short period was anticipated to present a unique challenge in the undeveloped and thickly vegetated, karst landscape of Little Cayman.

We were able to operate our system for the first 2 weeks. Unfortunately, a problem with the mechanical reliability of the tracking system led to a grounding of the system for the remainder of the field season. This did provide opportunity to not only evaluate our system during the first 2 weeks, but also directly compare the drone tracking system methodology and the manual tracking methodology in terms of effort and man-hours, as well as operational efficiency. We show the breakdown of transmitters tracked using the drone versus triangulation in Figure 6, where we can see that using the drone tracking system, we are able to hit a higher number of tracks per day as well as a higher average number of tracks per day (shown by the positive Y values). We were unable to sustain this pace (as

⁴<http://www.ettus.com/all-products/usrp-b200mini/>

⁵<http://lna4all.blogspot.com>

⁶<https://ark.intel.com/content/www/us/en/ark/products/96421/intel-joule-550x-compute-module.html>

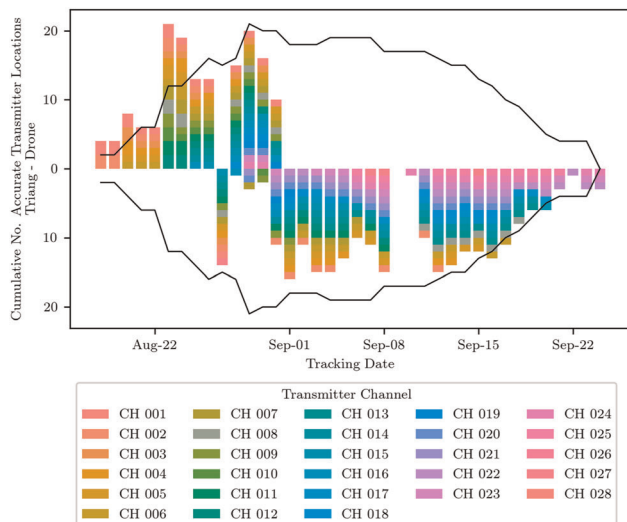


FIGURE 6 Cumulative number of transmitter localizations yielding coordinates with mean error <200 m between August 18 and September 24 on Little Cayman. The y-intercept differentiates points obtained by triangulation (Triang.) versus unmanned aerial vehicle. Different colors in the bars represent different transmitter channels in the data set. The mirrored line indicates the total number of transmitters for which tracking was actively being attempted on each tracking day [Color figure can be viewed at wileyonlinelibrary.com]

shown by the negative X values occurring on August 27 and after August 31) due to mechanical failures with the tracking system.

During the period between August 18 and 31, scientists released 20 of the study's 28 tracking subjects. Following the initial release, accurate transmitter locations (estimated to within 200 m; $n = 189$) were obtained every 0.49–1.35 days. The vast majority of these coordinates (81.5%) were obtained from UAV flights, and the mean precision of coordinates approximated by this method was 25.9 ± 25.25 m. During the period when the scientists were solely dependent on triangulation to estimate transmitter locations (September 1–24), estimates were significantly less precise (mean precision = 49.73 ± 49.8 m; $n = 209$; $p = 2.6e - 06$) and were obtained significantly less frequently (every 0.17–2.67 days; $t = -5.63$; $p = 1.04e - 07$). These results support the assertion that use of a UAV in a biological field study can help increase daily data collection and quality by reducing time requirements and increasing precision for the location of transmitter animals. Despite the clear advantages of UAV tracking over traditional methods, the scientists faced challenges with the technology. These included limitations that were shared with triangulation. For example, when animals moved outside the range at which an antenna could detect them, which occurred at distances as short as ≈ 200 m from the roadside in some areas of thick mangrove, narrowing the search area to the maximum grid size allowable by the UAV was not possible. Thus, many data points were lost when animals cut across the interior of the island.

It is important to note that this field deployment was not solely focused on testing the drone tracking system, but also on gathering

scientific data. During this field season, new insights into patterns of natal dispersal were gleaned from the combination of drone-based tracking and manual triangulation. For instance the greater frequency and precision of tracking facilitated by the UAV early in the season helped to illustrate that patterns of movement can vary remarkably among neonates even over short time frames (Moss et al., 2020). Characterizing fine-scale behavioral variation among neonates dispersing through different habitat types is of conservation importance because increased time spent in habitat such as mangrove has been shown to correlate with increased probability of survivorship (Knapp et al., 2010).

4.3 | Performance validation

We have discussed our system in detail and its performance in an actual field study. Finally, we would like to compare our system's performance in field tests with the performance reported by Nguyen, Dressel, and Cliff, as shown in Table 1. Note that these systems were not evaluated in actual field studies. Nevertheless, we want to compare the performance of our system side-by-side to provide context. While our system falls short of achieving the most precise estimates or the best flight time, it maintains a high level of performance throughout many trials, demonstrating robustness through field tests. In this comparison, we define flight time to be the time from takeoff to landing, or as reported by the authors, and mission time to be the time from takeoff to delivery of an estimate. For real-time systems, flight time and mission time are typically very similar, and differ only by the time needed for the operator to realize that the vehicle has reported an estimate, take control, and land the aircraft. For our data, we have averaged the data over all tracking missions flown during the 2017 Cayman Islands deployment.

In 2018, Nguyen tested a range-based particle filter system on a 3DR Iris⁷ and conducted a series of 16 flights to validate tracking performance. These flights were conducted in a search area of 75 m by 300 m on two humans carrying wildlife radio transmitters, launching from the southernmost corner of their search area. Their system reported a best root mean square estimate error of 22.7 ± 13.9 m in about 2.3 min (Nguyen et al., 2019). While our systems overall are similar, our overall mission times are typically longer. We attribute this to our mission times including time to transit to the survey area, postprocessing, and more in-depth data gathering. This a key difference between field tests and demonstrations—in the field, missions often take longer

TABLE 1 Comparison of approaches

System	Platform	Avg. precision (m)	Avg. mission time (s)	No. of trials
Nguyen	3DR Iris	22.7	135	16
Dressel	DJI M-100	5	37	3
Cliff	AT Falcon 8	51.47	600	8
Our System	3DR Solo	25.9	600	152

because the drone may need to start from a position well outside the payload's detection range of the target. In particular, the drone may need to start without being able to detect the target during launch.

In 2018, Dressel tested a bearing-based histogram filter system on a DJI M-100⁸ and conducted a series of flights to validate tracking performance. These flights were conducted in a search area of 400 m by 400 m on various RF sources, again starting from within the search area, and thus within detection range of the RF sources. Their system reported a fix when a 5 m by 5 m cell contained 50% confidence of estimation, which occurred in 37 s (Dressel & Kochenderfer, 2018). It is difficult to compare the estimated error, as we do not know the distribution of their estimation error, but Dressel does claim a faster time to estimate. Again, this can be attributed to our mission times including time to transit to the survey area. Our system is also significantly smaller, which enhances its applicability in the field.

Lastly, in 2018, Cliff field-tested a range- and bearing-based grid filter system on an Ascending Technologies Falcon 8,⁹ and conducted a series of eight flights to validate tracking performance on tagged swift parrots, also starting from within detection range. Their system reported a best estimate precision of 55 m in 10 min (Cliff et al., 2018). Our approach is able to generate a far more precise estimate in a similar overall time, with a much smaller airframe, however, the precision of Cliff's system may be worse due to their subject animals moving during their tests.

5 | CONCLUSION AND FUTURE WORK

As our collaboration with the SDZICR progresses, we anticipate adding features that will continue to make this system as efficient, accurate, reliable, and cost-effective as possible. Some of these features include online detection and estimation, intelligent path planning, and flight platform upgrades. In addition, we are redesigning the physical system to be more robust, so that it can stand up to field conditions. This will improve the usability of the system by further developing the automation and training for this system, and continuing to generate validation data to ensure that the estimation is robust.

Some specific changes we have already implemented and are currently testing are: new signal processing chain, new on-board computer, and real-time localization. As we continue to reanalyze the 2017 season data with the new signal processing chain, we are gaining a better understanding of the potential performance of this system. We deployed an updated and improved system to Big Ambergris Cay in the Turks and Caicos Islands during the summer of 2019, with promising improvements. We are looking to continue improvements on this system as new opportunities to test and deploy arrive.

We are continuing to redesign the flight system and physical payload for increased reliability against vibration, mishandling, and general wear

and tear, as these were the major factors that contributed to the inability of the system to sustain operations beyond 2 weeks. We are also redesigning the software architecture in the payload and ground control station to be able to recognize and handle failures while maintaining data integrity, so as to maximize the utility and reliability of the system, as these contributed to some of the decreases in our ability to track transmitters. Finally, we are continuing to improve the way that scientists interact with and utilize our system, which will permit increases in the amount of data that scientists can successfully gather in future deployments.

ACKNOWLEDGMENTS

We would like to thank Stesha Pasachnik (Fort Worth Zoo) for her assistance with the initial development of this project while a postdoctoral fellow with the San Diego Zoo Institute for Conservation Research, and Matthew Epperson (UC San Diego—Engineers for Exploration), George Waters (GWANDA), and the Cayman Islands Department of Environment for their support and assistance in making the development and deployment of this system in the Cayman Islands possible. We would also like to acknowledge the effort put in by the students in UC San Diego's Engineers for Exploration in supporting this project. This paper is based on work supported by the National Science Foundation under grants CNS-1544757, CNS-1560162, and CNS-1852403, the Qualcomm Institute at UC San Diego, the UC San Diego Frontiers of Innovation Scholars Program, the San Diego Zoo Institute for Conservation Research, Mississippi State University, and the Rufford Foundation.

DATA AVAILABILITY STATEMENT

The data that support the findings of this study are available from the corresponding author upon reasonable request.

REFERENCES

- Allen, A. M., & Singh, N. J. (2016). Linking movement ecology with wildlife management and conservation. *Frontiers in Ecology and Evolution*, 3, 155.
- Bayram, H., Stefas, N., & Isler, V. (2018). Aerial radio-based telemetry for tracking wildlife. *2018 IEEE/RSJ International Conference on Intelligent Robots and Systems (IROS)*.
- Cliff, O., Fitch, R., Sukkarieh, S., Saunders, D., & Heinsohn, R. (2015). Online localization of radio-tagged wildlife with an autonomous aerial robot system. *Robotics: Science and Systems XI*.
- Cliff, O. M., Saunders, D. L., & Fitch, R. (2018). Robotic ecology: Tracking small dynamic animals with an autonomous aerial vehicle. *Science Robotics*, 3(23), eaat8409. <https://doi.org/10.1126/scirobotics.aat8409>
- dos Santos, G. A. M., Barnes, Z., Lo, E., Ritoper, B., Nishizaki, L., Tejada, X., Ke, A., Lin, H., Schurgers, C., Lin, A., & Kastner, R. (2014). Small unmanned aerial vehicle system for wildlife radio collar tracking. *2014 IEEE 11th International Conference on Mobile Ad Hoc and Sensor Systems, Philadelphia, PA, USA*. <https://doi.org/10.1109/mass.2014.48>
- Dressel, L. K., & Kochenderfer, M. J. (2018). Efficient and low-cost localization of radio signals with a multirotor UAV. *2018 AIAA Guidance, Navigation, and Control Conference*.
- Gottwald, J., Zeidler, R., Friess, N., Ludwig, M., Reudenbach, C., & Naus, T. (2019). Introduction of an automatic and open-source radio-tracking system for small animals. *Methods in Ecology and Evolution*, 10(12), 2163–2172.

⁷Discontinued in 2015.

⁸<https://www.dji.com/matrice100>

⁹<http://www.asctec.de/en/uav-uas-drones-rpas-roav/asctec-falcon-8/>

- Gutierrez, J. (2008). Selected readings on telecommunications and networking. *Premier reference source*. IGI Global.
- Harris, S., Cresswell, W. J., Forde, P. G., Trehwella, W. J., Woollard, T., & Wray, S. (1990). Home-range analysis using radio-tracking data—a review of problems and techniques particularly as applied to the study of mammals. *Mammal Review*, 20(2–3), 97–123.
- Jensen, A., & Chen, Y. (2013). Tracking tagged fish with swarming unmanned aerial vehicles using fractional order potential fields and kalman filtering. *2013 International Conference on Unmanned Aircraft Systems (ICUAS)*.
- Kays, R., Tilak, S., Crofoot, M., Fountain, T., Obando, D., Ortega, A., Kuemmeth, F., Mandel, J., Swenson, G., Lambert, T., & Hirsch, B. (2011). Tracking animal location and activity with an automated radio telemetry system in a tropical rainforest. *The Computer Journal*, 54(12), 1931–1948.
- Kenward, R. (2007). *A manual for wildlife radio tagging*. Academic Press.
- Knapp, C. R., Alvarez-Clare, S., & Perez-Heydrich, C. (2010). The influence of landscape heterogeneity and dispersal on survival of neonate insular iguanas. *Copeia*, 2010(1), 62–70.
- Korner, F., Speck, R., Goktogan, A. H., & Sukkarieh, S. (2010). Autonomous airborne wildlife tracking using radio signal strength. *2010 IEEE/RSJ International Conference on Intelligent Robots and Systems*.
- Lascelles, B. G., Taylor, P. R., Miller, M. G. R., Dias, M. P., Oppel, S., Torres, L., Hedd, A., LeCorre, M., Phillips, R. A., Shaffer, S. A., Weimerskirch, H., & Small, C. (2016). Applying global criteria to tracking data to define important areas for marine conservation. *Diversity and Distributions*, 22(4), 422–431.
- Mech, L. D. (1986). *Handbook of animal radio-tracking*. University of Minnesota Press.
- Millsbaugh, J. J., & Marzluff, J. M. (2009). *Radio tracking and animal populations*. Academic Press.
- Moss, J. B., Gerber, G. P., Goetz, M., Haakonsson, J. E., Harvey, J. C., Laaser, T., & Welch, M. E. (2020). Contrasting patterns of movement across life stages in an insular iguana population. *Journal of Herpetology*, 54(1), 67–77.
- Nabeel, M., Bloessl, B., and Dressler, F. (2016). On using BOC modulation in ultra-low power sensor networks for wildlife tracking. *2016 IEEE Wireless Communications and Networking Conference* (pp. 1–6).
- Nguyen, H. V., Chesser, M., Koh, L. P., Rezatofighi, S. H., & Ranasinghe, D. C. (2019). Trackerbots: Autonomous unmanned aerial vehicle for real-time localization and tracking of multiple radio-tagged animals. *Journal of Field Robotics*, 36(3), 617–635.
- Pérez-Buitrago, N., & Sabat, A. (2007). Natal dispersal, home range and habitat use of hatchlings of the Mona Island iguana (*Cyclura cornuta stejnegeri*). *Applied Herpetology*, 2007(4), 365–376.
- Posch, A., & Sukkarieh, S. (2009). UAV based search for a radio tagged animal using particle filters. *Australasian Conference on Robotics and Automation (ACRA)*, Sydney, Australia.
- Santos, G. A. M. D., Barnes, Z., Lo, E., Ritoper, B., Nishizaki, L., Tejada, X., Ke, A., Lin, H., Schurgers, C., Lin, A., & Kastner, R. (2014). Small unmanned aerial vehicle system for wildlife radio collar tracking. *2014 IEEE 11th International Conference on Mobile Ad Hoc and Sensor Systems*.
- Soriano, P., Caballero, F., & Ollero, A. (2009). RF-based particle filter localization for wildlife tracking by using an UAV. *International Symposium on Robotics* (pp. 239–244).
- Vonehr, K., Hilaski, S., Dunne, B. E., & Ward, J. (2016). Software defined radio for direction-finding in uav wildlife tracking. *2016 IEEE International Conference on Electro Information Technology (EIT)*.
- Webber, D., Hui, N., Kastner, R., & Schurgers, C. (2017). Radio receiver design for unmanned aerial wildlife tracking. *2017 International Conference on Computing, Networking and Communications (ICNC)*.
- Whitaker, J. C. (2005). *The electronics handbook*. Taylor and Francis.
- White, G. C., & Garrott, R. A. (2012). *Analysis of wildlife radio-tracking data*. Academic Press.
- Wikelski, M., Kays, R. W., Kasdin, N. J., Thorup, K., Smith, J. A., & Swenson, G. W. (2007). Going wild: What a global small-animal tracking system could do for experimental biologists. *Journal of Experimental Biology*, 210(2), 181–186.

How to cite this article: Hui, N. T., Lo, E. K., Moss, J. B., Gerber, G. P., Welch, M. E., Kastner, R., & Schurgers, C. (2021). A more precise way to localize animals using drones. *Journal of Field Robotics*, 1–12.
<https://doi.org/10.1002/rob.22017>